

# 1D3V PIC simulation of propagation of relativistic electron beam in an inhomogeneous plasma

Chandrashekhara Shukla<sup>1,\*</sup>, Amita Das<sup>1</sup>, and Kartik Patel<sup>2</sup>

<sup>1</sup>*Institute for Plasma Research, Bhat, Gandhinagar - 382428, India and*

<sup>2</sup>*Bhabha Atomic Research Centre, Trombay, Mumbai - 400 085, India*

(Dated: March 5, 2022)

## Abstract

A recent experimental observation has shown efficient transport of Mega Ampere of electron currents through aligned carbon nanotube arrays [Phys. Rev Letts. **108**, 235005 (2012)]. The result was subsequently interpreted on the basis of suppression of the filamentation instability in an inhomogeneous plasma [Phys. Plasmas **21**, 012108 (2014)]. This inhomogeneity forms as a result of the ionization of the carbon nanotubes. In the present work a full 1D3V Particle-in-Cell (PIC) simulations have been carried out for the propagation of relativistic electron beams (REB) through an inhomogeneous background plasma. The suppression of the filamentation instability, responsible for beam divergence, is shown. The simulation also confirms that in the nonlinear regime too the REB propagation is better when it propagates through a plasma whose density is inhomogeneous transverse to the beam. The role of inhomogeneity scale length, its amplitude and the transverse beam temperature etc., in the suppression of the instability is studied in detail.

---

\* amita@ipr.res.in

## I. INTRODUCTION

The generation of relativistic electron beams (REB) through the interaction of a high power laser ( $I \geq 10^{19} \text{W/cm}^2$ ) with a solid target [1, 2] and its collimated propagation through a plasma is a topic of extensive studies due to its applications in cutting edge technologies, such as fast ignition scheme (FIS) [3] of laser fusion, compact particle acceleration [4], fast plasma switches [5] and laser induced radiation sources [6].

The transportation of an electron beam which carries a current much higher than the Alfvén current limit  $I = (mc^3/e)\gamma = 17\gamma_b k \text{ A}$ , ( $m$  is the electron mass,  $e$  is the electronic charge,  $c$  is speed of light and  $\gamma_b$  is the Lorentz factor of the beam) is not permitted due to its own strong magnetic field. However, in plasmas a spatially overlapping return shielding current by the background electrons inhibits the magnetic field generation and permits the propagation of beams with such high forward currents. The combination of the forward and return currents in plasmas are, however, susceptible to several instabilities viz., two-stream [7], Weibel [8], filamentation [9] and oblique modes [10]. The two-stream instability is a purely longitudinal electrostatic mode which generate density stripes perpendicular to the beam flow direction. The Weibel instability is purely transverse electromagnetic mode which occurs in the system due to the temperature anisotropy. This instability generates a magnetic field in the unmagnetized plasma system. A similar instability which generates a magnetic field in unmagnetized beam-plasma systems is known as the filamentation instability or beam-Weibel instability [11]. These instabilities have a detrimental influence on the propagation of the relativistic energy electron beam through a plasma and hence put practical constraints. In order to suitably utilize the relativistic electron beams these constraints on the propagation of beam through a plasma needs to be overcome. A lot of experimental, theoretical and simulation work has been devoted to control and suppress these instabilities [12–15]. The effect on the filamentation instability of beam density [16], beam velocity [16], transverse temperature [17] and collisions [18] has been widely studied. A recent experimental [19] result, has shown many fold improvement in the propagation of a hot relativistic electron beam through an array of carbon nanotubes (CNTs). An explanation of this has been put forth by Mishra *et al.* [20] suggesting that the inhomogeneous plasma created by the ionization of the CNTs by the front of the beam is responsible for the stabilization of transverse instabilities, thereby aiding the collimated propagation of the

beam through longer distances compared to a homogeneous plasma. Here we carry out the PIC simulations to study the role of inhomogeneity with arbitrary amplitude, on the propagation of electron beam through plasma.

The manuscript has been organized as follows. Section II contains the details of the model configuration and governing equations. In section III, the analytical results are presented. The details of PIC simulations are given in section IV. The observation of results from PIC simulation are presented in section V and it's interpretation are given in sec.VI. In last sec. VII, we conclude our results.

## II. MODEL CONFIGURATION AND GOVERNING EQUATIONS

The model configuration chosen for our studies has been shown in Fig. 1. The beam and the return current are chosen to flow along the  $\pm\hat{y}$  respectively. The ion density is chosen to have sinusoidal inhomogeneity along  $\hat{x}$  riding on a constant density of  $n_0$ . The amplitude of the inhomogeneity is  $\epsilon$  and the spatial variations are characterized by a wavenumber  $k_s = 2\pi/\lambda_s$  as shown in Fig. 1. The ions are considered to be at rest at such fast electron time scales and provide for charge neutralization as a background species. The density, velocity and temperature are denoted by  $n_\alpha$ ,  $v_\alpha$  and  $T_\alpha$ , with suffix  $\alpha$  standing for  $b$  (beam) and  $p$  ( background) plasma electrons respectively. The combination of the beam - plasma system can be represented by a coupled fluid Maxwell equations, with electrons contributing to forward and return currents treated as two distinct fluids. The normalized governing equation in such a case is:

$$\frac{\partial n_\alpha}{\partial t} + \nabla \cdot (n_\alpha \vec{v}_\alpha) = 0 \quad (1)$$

$$\frac{\partial \vec{p}_\alpha}{\partial t} + \vec{v}_\alpha \cdot \nabla \vec{p}_\alpha = - \left( \vec{E} + \vec{v}_\alpha \times \vec{B} \right) - \frac{\nabla P_\alpha}{n_\alpha} \quad (2)$$

$$\frac{\partial \vec{B}}{\partial t} = -\nabla \times \vec{E} \quad (3)$$

$$\frac{\partial \vec{E}}{\partial t} = \nabla \times \vec{B} - \Sigma_\alpha \vec{J}_\alpha \quad (4)$$

with  $\vec{v}_\alpha = \vec{p}_\alpha / (1 + p_\alpha^2)^{\frac{1}{2}}$ ,  $\vec{J}_\alpha = -n_\alpha \vec{v}_\alpha$ . The pressure  $P_\alpha$  is provided by the equation of state. In the above equations, velocity is normalized by speed of light  $c$ , density by  $n_0$ , frequency by  $\omega_0 = 4\pi n_0 e^2 / m_e$  and electric and magnetic field by  $E_0 = B_0 = m_e c \omega_0 / e$  where  $m_e$  is electron rest mass and  $e$  is electron charge.

In the equilibrium there is no electric and magnetic field, so there is complete charge as well as current neutralization. This is achieved by balancing the forward and return electron currents at each spatial location. The total charge density due to electrons is balanced by the background ion charge density. The background plasma has been chosen cold ( $T_{0p} = 0$ ) in all our analytical as well as in simulation studies. The profile of transverse temperature  $T_\alpha$  in beam is chosen in such a way that gradient of pressure is zero in equilibrium. The temperature parallel to beam propagation direction is chosen to be zero. Thus, for an inhomogeneous beam plasma system considered by us in this work we have the following conditions for equilibrium:

$$n_{0i}(x) = n_{0b}(x) + n_{0p}(x) \quad (5)$$

$$\Sigma_\alpha n_{0\alpha}(x) v_{0\alpha} = 0 \quad (6)$$

In equilibrium beam pressure  $P_{0b}$  is chosen to be independent of  $x$ . This is achieved by choosing the beam temperature  $T_{0b}(x)$  to satisfy the following condition

$$P_{0b} = T_{0b}(x) n_{0b}(x) = \text{constant} = k. \quad (7)$$

$$T_{0b}(x) = k/n_{0b}(x) \quad (8)$$

The suffix 0 indicates the equilibrium fields. This choice is very artificial construct, However it has been chosen to satisfy the equilibrium conditions so that comparisons with simulation can be made. We linearize the equations (1)-(5) to obtain linear growth rate of instability. For the inhomogeneous case the equation cannot be Fourier analyzed in  $x$  and the eigen value can be determined by solving following coupled set of differential equations:

$$\begin{aligned} \omega \gamma_{0\alpha} v''_{l\alpha y} + \omega^3 \gamma_{0\alpha}^3 v_{l\alpha y} - \omega \Sigma_\alpha n_{0\alpha} v_{l\alpha y} + i \Sigma_\alpha v_{0\alpha y} (n_{0\alpha} v_{l\alpha x})' &= 0 \quad (9) \\ \eta T_{0\alpha} v''_{l\alpha x} + \left( 2 \frac{\eta T_{0\alpha}}{n_{0\alpha}} n'_{0\alpha} + \eta T'_{0\alpha} \right) v_{l\alpha x}' + \left( \frac{\eta T_{0\alpha}}{n_{0\alpha}} n''_{0\alpha} + \eta \frac{T'_{0\alpha}}{n_{0\alpha}} n'_{0\alpha} + \omega^2 \gamma_{0\alpha} \right) v_{l\alpha x} - \Sigma_\alpha n_{0\alpha} v_{l\alpha x} \\ + i \omega \gamma_{0\alpha}^3 v_{0\alpha y} v'_{l\alpha y} &= 0 \quad (10) \end{aligned}$$

Where  $\eta$  is ratio of specific heat. For the case of homogeneous plasma, eq. (9) and eq. (10) reduce to

$$\omega \gamma_{0\alpha} v''_{l\alpha y} + \omega^3 \gamma_{0\alpha}^3 v_{l\alpha y} - \omega \Sigma_\alpha n_{0\alpha} v_{l\alpha y} + i \Sigma_\alpha v_{0\alpha y} n_{0\alpha} v'_{l\alpha x} = 0 \quad (11)$$

$$\eta T_{0\alpha} v''_{l\alpha x} + \omega^2 \gamma_{0\alpha} v_{l\alpha x} - \Sigma_\alpha n_{0\alpha} v_{l\alpha x} + i \omega \gamma_{0\alpha}^3 v_{0\alpha y} v'_{l\alpha y} = 0 \quad (12)$$

By taking Fourier transform in  $x$ , we obtain the following standard dispersion relation

$$\begin{aligned} & \left( \omega^2 - k_x^2 - \sum_{\alpha} \frac{n_{0\alpha}}{\gamma_{0\alpha}^3} \right) \left( \omega^4 \gamma_{0b} \gamma_{0p} - \omega^2 \gamma_{0b} \gamma_{0p} \sum_{\alpha} \frac{n_{0\alpha}}{\gamma_{0\alpha}} - \eta T_{0b} k_x^2 (\omega^2 \gamma_{0p} - n_{0p}) \right) \\ & - k_x^2 \left( \omega^2 \gamma_{0b} \gamma_{0p} \sum_{\alpha} \frac{n_{0\alpha} v_{0\alpha}^2}{\gamma_{0\alpha}} - n_{0p} n_{0b} \sum_{\alpha} v_{0\alpha}^2 + 2n_{0p} n_{0b} v_{0p} v_{0b} - \eta T_{0b} k_x^2 n_{0p} v_{0p}^2 \right) = 0 \end{aligned} \quad (13)$$

This equation contains two oscillatory mode and one purely growing electromagnetic mode which is known as filamentation or Weibel instability.

### III. ANALYTICAL STUDIES

For analytical tractability of the inhomogeneous problem a choice of sinusoidal variation riding on a homogeneous background density such as

$$n_{0i} = [1 + \varepsilon \cos(k_s x)] \quad (14)$$

is chosen. Here  $\varepsilon$  is the inhomogeneity amplitude and  $k_s = 2\pi m/L_x$  ( $m$  is an integer) is the inhomogeneity wave number with  $L_x$  as the system length. To satisfy the quasi-neutrality condition the equilibrium beam and plasma density is chosen as

$$\begin{aligned} n_{0b} &= \beta(1 + \varepsilon \cos(k_s x)) \\ n_{0p} &= (1 - \beta)(1 + \varepsilon \cos(k_s x)) \end{aligned} \quad (15)$$

where  $\beta$  is a fraction. Now choosing the perturbed fields as  $f_{\alpha} = \sum_j^{\dots, \pm 2, \pm 1, 0} f_{\alpha j} e^{i((k+jk_s)x - \omega t)}$  and assuming  $\varepsilon$  to be small so that retaining only the first order terms (as done in the paper by Mishra *et al.* [20]), we can evaluate the growth rate. We evaluate the growth rate  $\Gamma_{gr}$  as a function of  $k$ , using the same method. The plots shown in Fig. 2 compare the growth rates for the homogeneous case with inhomogeneous cases. Fig. 2 (a), we plot the growth rate  $\Gamma_{gr}$  versus wave vector  $k$  for a homogeneous (solid line) and inhomogeneous cold beam plasma system for  $\varepsilon=0.1$ , for  $k_s = \pi(-)$ ,  $2\pi(-.-)$  and  $3\pi(*).$  The other parameters are  $n_{0b}/n_{0p} = 1/9$  or  $n_{0b}/n_{0e} = 0.1$ ,  $v_{0b} = 0.9c$ ,  $v_{0p} = -0.1c$ ,  $T_{0b} = 0$ ,  $T_{0p} = 0$ . From this plot we can see that for the homogeneous case, the  $\Gamma_{gr}$  increases with  $k$  for small values of  $k$  and saturates at  $k \simeq 3$ . However, for the inhomogeneous case ( $\varepsilon=0.1$ )  $\Gamma_{gr}$  for small values of  $k$  is large compared to the homogeneous one. The increase in  $\Gamma_{gr}$  with  $k$  is very mild and ultimately there is a saturation at higher  $k$  values. The maximum value of the growth rate  $\Gamma_{gr}$  increases

with  $k_s$  for a cold system. The effect of transverse beam temperature ( $T_{0b\perp} = 10$  keV) over the growth rate can be seen in Fig. 2(b). The growth rate  $\Gamma_{gr}$  of the homogeneous hot beam and cold background plasma system (solid line) increases with  $k$  for small values of  $k$  but starts decreasing after  $k > 0.5$  and completely stabilizes at higher wave numbers ( $k > 1$ ). The effect of inhomogeneity on the hot beam and cold background plasma can be seen in Fig. 2(b) and Fig. 2(c). The Fig. 2(b) illustrate the effect of inhomogeneity scale length  $k_s$  over the  $\Gamma_{gr}$  at fixed value of  $\varepsilon$ . We see that for  $\varepsilon = 0.1$  and  $k_s = \pi$  (which is  $\lambda_s > c/\omega_p$ ), the instability domain of  $\Gamma_{gr}$  is much larger compared to the homogeneous case. It is also observed that when the inhomogeneity scale length is further reduced to half, i.e.  $k_s = 2\pi(-\infty)$  for  $\varepsilon = 0.1$ , the instability is suppressed for all values of  $k$ . In Fig. 2(c), we plot the growth rate  $\Gamma_{gr}$  versus wave vector  $kc/\omega_p$  to see the effect of  $\varepsilon$  on  $\Gamma_{gr}$  at  $T_{0b\perp} = 10$  keV. We see that  $\Gamma_{gr}$  reduces with increasing  $\varepsilon$ . Thus the study shows that at finite transverse beam temperature the effect of increasing  $k_s$  as well as  $\varepsilon$  is to stabilize the Weibel instability. In Table - I we have tabulated the value of maximum growth rate for various cases.

**TABLE I**

The maximum growth rate of filamentation instability evaluated analytically under the approximation of weak inhomogeneity amplitude.

| $T_{0b\perp}(keV)$ | $\varepsilon$ | $k_s$  | $\Gamma_{gr}(\text{max.})$ |
|--------------------|---------------|--------|----------------------------|
| 0.0                | 0.0           | 0.0    | 0.2006                     |
| 0.0                | 0.1           | $\pi$  | 0.2057                     |
| 0.0                | 0.1           | $2\pi$ | 0.2074                     |
| 0.0                | 0.1           | $3\pi$ | 0.2085                     |
| 10.0               | 0.0           | 0.0    | 0.0840                     |
| 10.0               | 0.1           | $\pi$  | 0.0831                     |
| 10.0               | 0.1           | $2\pi$ | 0.0770                     |
| 10.0               | 0.1           | $3\pi$ | 0.0094                     |
| 10.0               | 0.2           | $3\pi$ | 0.0000                     |

It is thus noted that for cold beam there is no significant difference between the growth rates of homogeneous and inhomogeneous cases except at long wavelengths. However, when the beam temperature is chosen as finite the growth rate for the inhomogeneous case significantly reduces with increasing  $k_s$  as well as  $\varepsilon$ . We feel that the reduction in growth rate

is responsible for transport over long distances observed in targets that had carbon nanotubes attached to them in experiments. The analytical inference is further corroborated by Particle - In- Cell (PIC) simulations. The results of PIC studies are presented in the next section.

#### IV. PIC SIMULATION DETAILS

We have performed Particle-In-Cell simulation to study the propagation of beam in both homogeneous and inhomogeneous plasma systems. The PIC code PICPSI3D used for this simulation has been developed indigenously by one of the authors (Kartik patel) [21] and has been used in several studies in the past [22]. The PICPSI3D was generalized by us to study the propagation of electron beam in an inhomogeneous plasma system. Only one dimensional variation in space (perpendicular to the beam propagation) has been chosen for our numerical studies here, for the purpose of comparison with recently carried out analytical linear studies.

The ions are not allowed to move in the simulations and merely provide a neutralizing background for the plasma. This makes the simulation faster and is a valid approximation to study the fast electron time scale phenomena of interest. The uniform plasma density  $n_0$  is chosen to be  $10n_c$  where  $n_c = 1.1 \times 10^{21} cm^{-3}$  is the critical density for  $1\mu m$  wavelength of laser light. The spatial simulation box length  $L_x = 60 c/\omega_0$ , where  $c/\omega_0 = d_e = 5.0 \times 10^{-2} \mu m$  is the skin depth corresponding to the density  $n_0$ . The one dimensional simulation box is divided in 6000 cells. The grid size is therefore equal to  $0.01 d_e$ . Thus, scales shorter than the skin depth can be resolved. The total number of electrons and ions chosen for the simulations are 1800000 each. This number represents the sum of background  $n_{0p}$  and beam  $n_{0b}$  electrons. The choice of inhomogeneous ion density and the separation between the two electron species of beam and background are made as per Eq.(14) and Eq.(15)

The beam temperature  $T_{b0\perp}$  is chosen to be finite in perpendicular direction according to Eq.(8). The time step is decided by the Courant condition. The charge neutrality as well as the null value of total current density is ensured initially. The considered system is also field free initially as required by equilibrium configuration. the system has an equilibrium configuration initially.

## V. SIMULATION OBSERVATIONS

For the homogeneous plasma density case (e.g.  $\epsilon = 0.0$ ,  $k_s = 0.0$ ) the system is plagued by the usual Weibel instability. This causes spatial separation between the forward and reverse electron currents. The separation leads to finite current density in space resulting in the growth of magnetic field energy. The evolution of box averaged magnetic field energy normalized by  $E_0^2 = (m_e c \omega_0 / e)^2$  energy of system is shown in Fig. 3 (b), Fig. 4 (b) and Fig. 5 (b). After an initial transient the curve settles down to a linear regime and subsequently shows saturation.

The slope of the linear portion of the main curve has been employed for the evaluation of the growth rate of the maximally unstable mode in the simulation. The growth rate has been tabulated in Table - II for various cases of parameters.

**TABLE II:**

The maximum growth rate of filamentation instability calculated from PIC simulation.

| $T_{0b\perp}(keV)$ | $\epsilon$ | $k_s$  | $\Gamma_{gr}(\text{max.})$ |
|--------------------|------------|--------|----------------------------|
| 0.0                | 0.0        | 0.0    | 0.2000                     |
| 0.0                | 0.1        | $2\pi$ | 0.2000                     |
| 0.0                | 0.1        | $3\pi$ | 0.2000                     |
| 10.0               | 0.0        | 0.0    | 0.0508                     |
| 10.0               | 0.1        | $2\pi$ | 0.0349                     |
| 10.0               | 0.1        | $3\pi$ | 0.0333                     |
| 10.0               | 0.2        | $2\pi$ | 0.0173                     |
| 10.0               | 0.2        | $3\pi$ | 0.0109                     |

From the table as well as by following the complete evolution it is evident that when the transverse temperature of the beam electrons is zero the inhomogeneous density causes no change. With increasing value of  $\epsilon$  and  $k_s$  the growth rate decreases when the temperature of the beam and background electrons is finite. This trend is similar to the behavior of growth rate evaluated analytically, shown in Table - I. When the plasma density is homogeneous the value of the growth rates evaluated analytically and through simulations are in good agreement. However, in the presence of inhomogeneity there is a small disagreement between



the quantitative values. This can be attributed to the approximate nature of the analytical treatment, wherein the inhomogeneity amplitude was assumed to be weak.

From Figures 3 (a), 4 (a) and 5 (a) it can also be seen that along with the growth of magnetic field energy, electrostatic field energy also grows. The development of an electric field directed along  $x$  during the course of simulation is responsible for this electrostatic energy. This electrostatic field develops as a result of the redistribution and bunching of electron charges in physical  $x$  space. It can be seen from the phase space plots of Figs. 6 and 9 that the electrons do reorganize in physical space. Furthermore, the locations where these electrons get accumulated are the regions with maximal currents and negligible magnetic and electric field as can be seen from Fig. 7

Finally we provide a comparison between the cases of homogeneous and inhomogeneous plasmas. It should be noted that the typical scale length of the magnetic field developed during the initial phase in the homogeneous case (Fig. 8 (a)) is of the order of the background plasma skin depth (e.g.  $5.33 \times 10^{-2} \mu m$ ). For the inhomogeneous case, the scale length of the magnetic field matches initially with the inhomogeneity scale length defined by the choice of  $k_s$  (Fig. 8 (b))(provided the scale length of inhomogeneity is smaller than the skin depth) else it is determined by the typical value of skin depth. At later stages (the nonlinear phase of the instability), however, the magnetic structures coalesce and acquire long scales typically comparable to simulation box size in both homogeneous (Fig. 8 (c)) and in-homogeneous (Fig. 8 (d)) (provided the growth rate remains finite in this case) cases.

To summarize the main observations are: (i) the inhomogeneous density causes no significant difference in the growth rate when the transverse temperature is chosen to be zero. (ii) the growth rate of the Weibel instability in the inhomogeneous density case is reduced compared to the homogeneous case when the transverse beam temperature is finite, (iii) The momentum  $p_x$  is typically quite large for beam electrons compared to the background plasma electrons. (iv) in the nonlinear regime the typical profile of electrostatic field created due to electron bunching in  $x$  is similar to that of the magnetic field. The zeros of both the fields coincide with each other in space and it is these very locations where electron bunching is observed.

## VI. INTERPRETATION OF NUMERICAL OBSERVATIONS

We now provide a simplified understanding of the observations made by PIC simulations listed out in previous section. In order to understand these results we consider the 1-D limit (with only variations along  $x$  being permitted) of the two fluid system of beam and background electrons described in section II. In 1-D the momentum equations of the two electron species from Eqs.(1) are:

$$\frac{dp_{xb}}{dt} = - \left[ -\frac{\partial\phi}{\partial x} + v_{yb}B_z \right] - \frac{1}{n_b} \frac{\partial P_b}{\partial x} \quad (16)$$

$$\frac{dp_{xp}}{dt} = - \left[ -\frac{\partial\phi}{\partial x} + v_{yp}B_z \right] \quad (17)$$

$$\frac{dp_{yb}}{dt} = - \left[ -\frac{\partial A_y}{\partial t} - v_{xb}B_z \right] \quad (18)$$

$$\frac{dp_{yp}}{dt} = - \left[ -\frac{\partial A_y}{\partial t} - v_{xp}B_z \right] \quad (19)$$

$$(20)$$

Here  $p_{i\alpha}$  for  $i = x$  and  $i = y$  corresponds to the  $x$  and  $y$  component of momentum respectively for the beam  $\alpha = b$  or plasma  $\alpha = p$  electrons. Also  $v_{i\alpha} = p_{i\alpha}/\gamma_\alpha$  (with  $\gamma_\alpha$  being the relativistic factor) is the corresponding velocity. Here  $P_b$  represents the transverse pressure which is zero for the case when the system is cold. The scalar and vector potentials are represented by  $\phi$  and  $\vec{A}$  respectively. In 1-D only  $A_y$  component is finite. Thus the only finite component of magnetic field is along  $\hat{z}$  and  $B_z = \partial A_y/\partial x$ .

The continuity equation can be written as

$$\frac{\partial n_\alpha}{\partial t} + \vec{v}_{x\alpha} \frac{\partial n_\alpha}{\partial x} + n_\alpha \frac{\partial v_{x\alpha}}{\partial x} = 0 \quad (21)$$

The Maxwell's equation become

$$\frac{\partial^2 \phi}{\partial x^2} = (\delta n_b + \delta n_p) \quad (22)$$

$$\frac{\partial^2 A_y}{\partial t^2} = \frac{\partial B_x}{\partial x} - [n_b v_{yb} + n_p v_{yp}] \quad (23)$$

Here  $n_b$  and  $n_p$  are the total densities of the beam and plasma electrons and  $\delta n_b$  and  $\delta n_p$  is the difference between the total and equilibrium densities respectively. If one considers the transverse temperature to be zero, the linearization of the above set of equations has no other term dependent on the electron densities except for  $E_x = -\partial\phi/\partial x$  in the momentum

equation. However, Weibel being primarily an electromagnetic instability the electrostatic field is very weak. Thus, the predominant term in the momentum equation is due to second term of  $v_{y0b}B_z$ , which is not influenced by the electron density. Thus, in the limit of zero temperature the homogeneous and inhomogeneous cases do not show any significant difference.

When the transverse temperature is finite our simulations show reduction in the Weibel growth rate. In this case the pressure term in Eq.(13) is effective and depends on the density inhomogeneity. It has been shown by an approximate analytical studies in [20] repeated and presented by us in Fig.2 that the growth rate indeed decreases in the inhomogeneous case. This is the main result of our simulations which qualitatively verifies the approximate results of [20]. This can also be relevant for the observed propagation of electrons over long distances in the presence of nanowires/nanotubes in experiments[19].

As we have stated earlier along with the development of magnetic field an electrostatic field also develops. This happens due to the bunching of electron densities at the location of zero magnetic field as shown in Fig. 7. At the location of zero magnetic field the perturbed density shows a maxima and the electric field also passes through zero. This arrangement is self consistent. The Lorentz force at these locations vanishes and hence a particle has a greater probability to accumulate over there. The location of maximum accumulation of electron density in turn results in the vanishing of the second derivative of electric field and for a Fourier spectrum this location should correspond to the zero of electric field.

## VII. SUMMARY AND CONCLUSION

We have shown through 1D3V PIC simulations that the growth rate of Weibel instability gets reduced in the presence of density inhomogeneity. This has relevance to a recent experimental observation of efficient transport of Mega Ampere of electron currents through aligned carbon nanotube arrays. The ionization of the carbon nanotubes by the front of laser pulse produces the plasma which has inhomogeneous density. Since the Weibel instability gets suppressed in such a inhomogeneous plasma, the current separation is reduced leading to the propagation of beam electrons over large distances.

This mechanism of efficient electron transport was earlier invoked by Mishra *et al.* [20] wherein it was shown analytically using two fluid description that the Weibel instability

gets suppressed. The present work supplements it with PIC studies. Our PIC simulations support the analytical observations qualitatively. The quantitative values of the growth rate differ slightly showing the approximate nature of the analysis.

**Acknowledgement:** We thank S. Mishra for many useful discussions.

- 
- [1] G. Malka and J. L. Miquel. Experimental confirmation of ponderomotive-force electrons produced by an ultrarelativistic laser pulse on a solid target. *Phys. Rev. Lett.*, 77:75–78, Jul 1996.
- [2] K. B. Wharton, S. P. Hatchett, S. C. Wilks, M. H. Key, J. D. Moody, V. Yanovsky, A. A. Offenberger, B. A. Hammel, M. D. Perry, and C. Joshi. *Phys. Rev. Lett.*, 81:822–825, Jul 1998.
- [3] M. Tabak, D. S. Clark, S. P. Hatchett, M. H. Key, B. F. Lasinski, R. A. Snavely, S. C. Wilks, R. P. J. Town, R. Stephens, E. M. Campbell, R. Kodama, K. Mima, K. A. Tanaka, S. Atzeni, and R. Freeman. Review of progress in fast ignitiona). *Physics of Plasmas*, 12(5), 2005.
- [4] A. J. Mackinnon, Y. Sentoku, P. K. Patel, D. W. Price, S. Hatchett, M. H. Key, C. Andersen, R. Snavely, and R. R. Freeman. Enhancement of proton acceleration by hot-electron recirculation in thin foils irradiated by ultraintense laser pulses. *Phys. Rev. Lett.*, 88:215006, May 2002.
- [5] J. Fuchs, J. C. Adam, F. Amiranoff, S. D. Baton, P. Gallant, L. Gremillet, A. Héron, J. C. Kieffer, G. Laval, G. Malka, J. L. Miquel, P. Mora, H. Pépin, and C. Rousseaux. Transmission through highly overdense plasma slabs with a subpicosecond relativistic laser pulse. *Phys. Rev. Lett.*, 80:2326–2329, Mar 1998.
- [6] H.-S. Park, D. M. Chambers, H.-K. Chung, R. J. Clarke, R. Eagleton, E. Giraldez, T. Goldsack, R. Heathcote, N. Izumi, M. H. Key, J. A. King, J. A. Koch, O. L. Landen, A. Nikroo, P. K. Patel, D. F. Price, B. A. Remington, H. F. Robey, R. A. Snavely, D. A. Steinman, R. B. Stephens, C. Stoeckl, M. Storm, M. Tabak, W. Theobald, R. P. J. Town, J. E. Wickersham, and B. B. Zhang. High-energy k radiography using high-intensity, short-pulse lasers. *Physics of Plasmas*, 13(5), 2006.
- [7] D. Bohm and E. P. Gross. Theory of plasma oscillations. a. origin of medium-like behavior. *Phys. Rev.*, 75:1851–1864, Jun 1949.
- [8] Erich S. Weibel. Spontaneously growing transverse waves in a plasma due to an anisotropic velocity distribution. *Phys. Rev. Lett.*, 2:83–84, Feb 1959.
- [9] Burton D. Fried. Mechanism for instability of transverse plasma waves. *Physics of Fluids*, 2(3):337–337, 1959.

- [10] F. Califano, R. Prandi, F. Pegoraro, and S. V. Bulanov. Nonlinear filamentation instability driven by an inhomogeneous current in a collisionless plasma. *Phys. Rev. E*, 58:7837–7845, Dec 1998.
- [11] Jeremy Martin Hill, Michael H. Key, Stephen P. Hatchett, and Richard R. Freeman. Beam-weibel filamentation instability in near-term and fast-ignition experiments. *Physics of Plasmas*, 12(8), 2005.
- [12] A. R. Bell and R. J. Kingham. Resistive collimation of electron beams in laser-produced plasmas. *Phys. Rev. Lett.*, 91:035003, Jul 2003.
- [13] A. P. L. Robinson, M. Sherlock, and P. A. Norreys. Artificial collimation of fast-electron beams with two laser pulses. *Phys. Rev. Lett.*, 100:025002, Jan 2008.
- [14] B. Ramakrishna, S. Kar, A. P. L. Robinson, D. J. Adams, K. Markey, M. N. Quinn, X. H. Yuan, P. McKenna, K. L. Lancaster, J. S. Green, R. H. H. Scott, P. A. Norreys, J. Schreiber, and M. Zepf. Laser-driven fast electron collimation in targets with resistivity boundary. *Phys. Rev. Lett.*, 105:135001, Sep 2010.
- [15] P. McKenna, A. P. L. Robinson, D. Neely, M. P. Desjarlais, D. C. Carroll, M. N. Quinn, X. H. Yuan, C. M. Brenner, M. Burza, M. Coury, P. Gallegos, R. J. Gray, K. L. Lancaster, Y. T. Li, X. X. Lin, O. Tresca, and C.-G. Wahlström. Effect of lattice structure on energetic electron transport in solids irradiated by ultraintense laser pulses. *Phys. Rev. Lett.*, 106:185004, May 2011.
- [16] Roswell Lee and Martin Lampe. Electromagnetic instabilities, filamentation, and focusing of relativistic electron beams. *Phys. Rev. Lett.*, 31:1390–1393, Dec 1973.
- [17] Lus O. Silva, Ricardo A. Fonseca, John W. Tonge, Warren B. Mori, and John M. Dawson. On the role of the purely transverse weibel instability in fast ignitor scenarios. *Physics of Plasmas*, 9(6), 2002.
- [18] Anupam Karmakar, Naveen Kumar, Alexander Pukhov, O. Polomarov, and Gennady Shvets. Detailed particle-in-cell simulations on the transport of a relativistic electron beam in plasmas. *Phys. Rev. E*, 80:016401, Jul 2009.
- [19] Gourab Chatterjee, Prashant Kumar Singh, Saima Ahmed, A. P. L. Robinson, Amit D. Lad, Sudipta Mondal, V. Narayanan, Iti Srivastava, Nikhil Koratkar, John Pasley, A. K. Sood, and G. Ravindra Kumar. Macroscopic transport of mega-ampere electron currents in aligned carbon-nanotube arrays. *Phys. Rev. Lett.*, 108:235005, Jun 2012.

- [20] S. K. Mishra, Predhiman Kaw, A. Das, S. Sengupta, and G. Ravindra Kumar. Stabilization of beam-weibel instability by equilibrium density ripples. *Physics of Plasmas* , 21(1), 2014.
- [21] B. S. Rao P. A. Naik P. D. Gupta A. Upadhyay, K. Patel. Three dimensional simulation of laserplasma based electron acceleration. *PRAMANA - Journal of Physics*, 78(4), 2012.
- [22] Ujjwal Sinha. Multistage ion acceleration in finite overdense target with a relativistic laser pulse. *Physics of Plasmas* , 20(7), 2013.

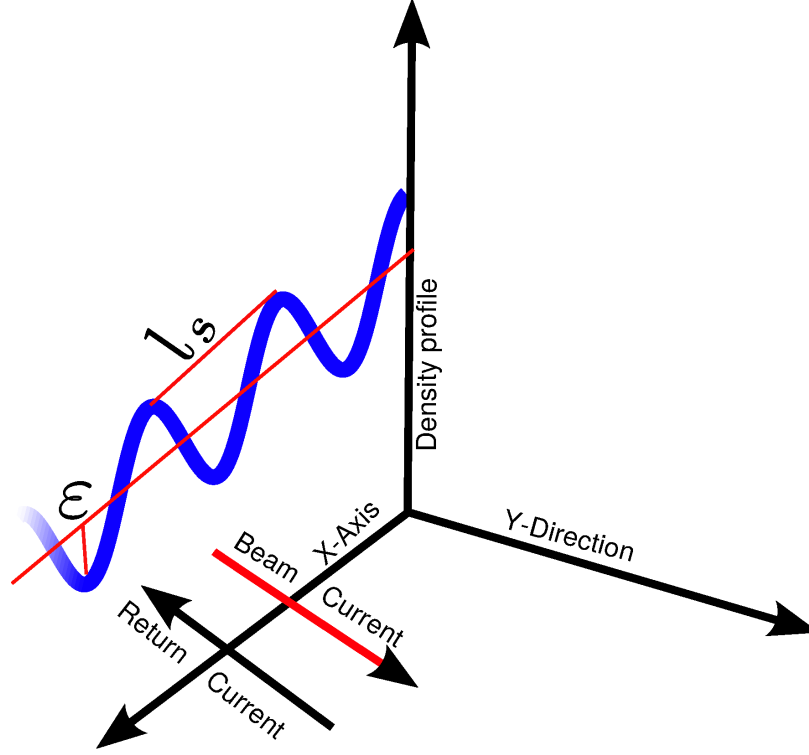


FIG. 1: schematic of model configuration

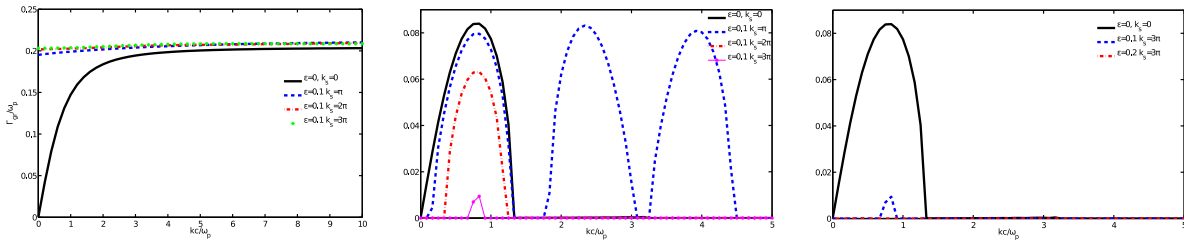


FIG. 2: Growth rate of the 1D filamentation instability versus the wave number  $k$  for a homogeneous and inhomogeneous beam-plasma: (a) shows growth rate for cold homogeneous beam-plasma system (solid line), for parameters  $n_{0b}/n_{0e} = 0.1$ ,  $v_{0b} = 0.9c$ ,  $v_{0p} = -0.1c$  and for inhomogeneous,  $\varepsilon=0.1$  at  $k_s=\pi(-)$ ,  $k_s=\pi(-)$  and  $k_s=\pi(*)$ . (b) at transverse beam temperature  $T_{b0\perp}=10$  keV, homogeneous (solid black), inhomogeneous for  $\varepsilon=0.1$  at  $k_s=\pi(-)$ ,  $2\pi(-)$  and  $3\pi(-)$  (c) at transverse beam temperature  $T_{b0\perp}=10$  keV, homogeneous (solid black), inhomogeneous at  $k_s=3\pi$  for  $\varepsilon=0.1(-)$  and  $0.2(-)$



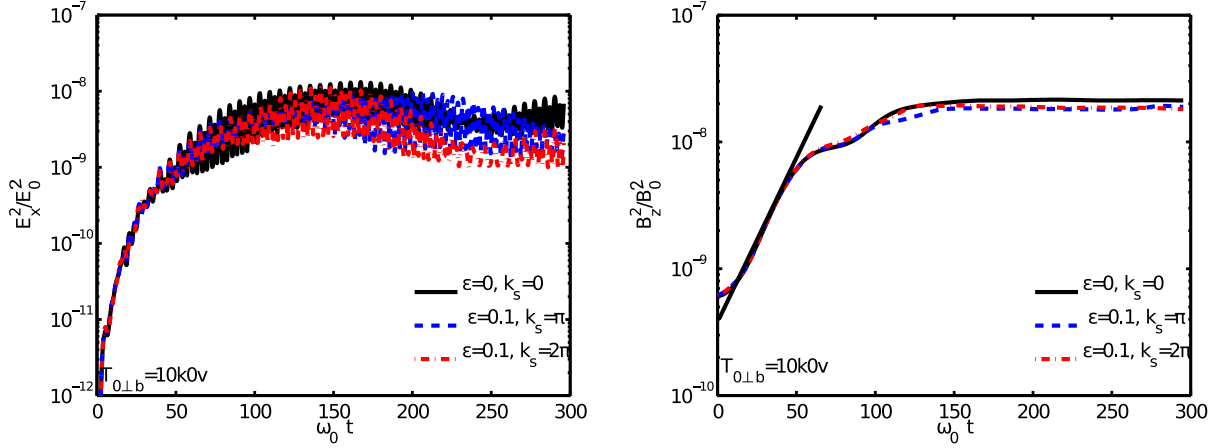


FIG. 3: Temporal evolution of the field energy densities for cold homogeneous and inhomogeneous beam-plasma simulation. (a) normalized electrostatic x-component of electric field energy (b) normalized z-component of magnetic field energy

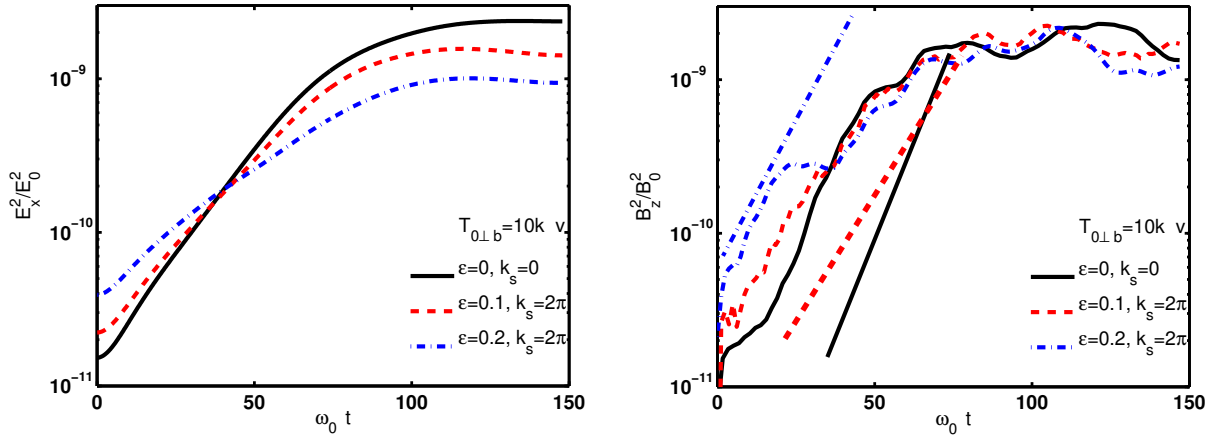


FIG. 4: Temporal evolution of the field energy densities for hot ( $T_{b0\perp}=10$  keV ) homogeneous and inhomogeneous beam-plasma simulation. (a) normalized electrostatic x-component of electric field energy  $E_x^2$  for  $\varepsilon=0$ ,  $k_s=0$  and  $\varepsilon=0.1$  and  $0.2$  for  $k_s=2\pi$  (b) normalized z-component of magnetic field energy  $B_z^2$  for  $\varepsilon=0$ ,  $k_s=0$  and  $\varepsilon=0.1$  and  $0.2$  for  $k_s=2\pi$

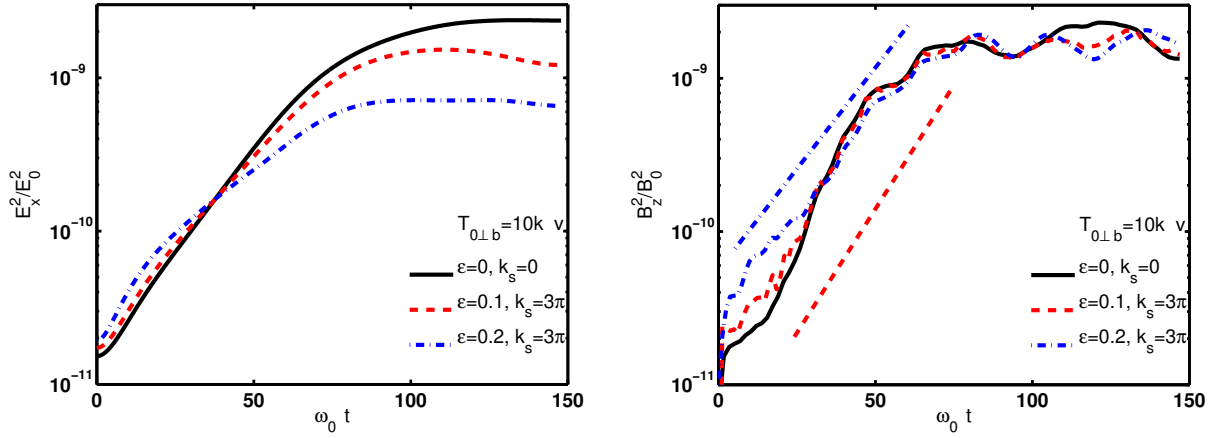


FIG. 5: Temporal evolution of the field energy densities for hot ( $T_{b0\perp}=10\text{keV}$ ) homogeneous and inhomogeneous beam-plasma simulation. (a) normalized electrostatic x-component of electric field energy  $E_x^2$  for  $\epsilon=0, k_s=0$  and  $\epsilon=0.1$  and  $0.2$  for  $k_s=3\pi$  (b) normalized z-component of magnetic field energy  $B_z^2$  for  $\epsilon=0, k_s=0$  and  $\epsilon=0.1$  and  $0.2$  for  $k_s=3\pi$

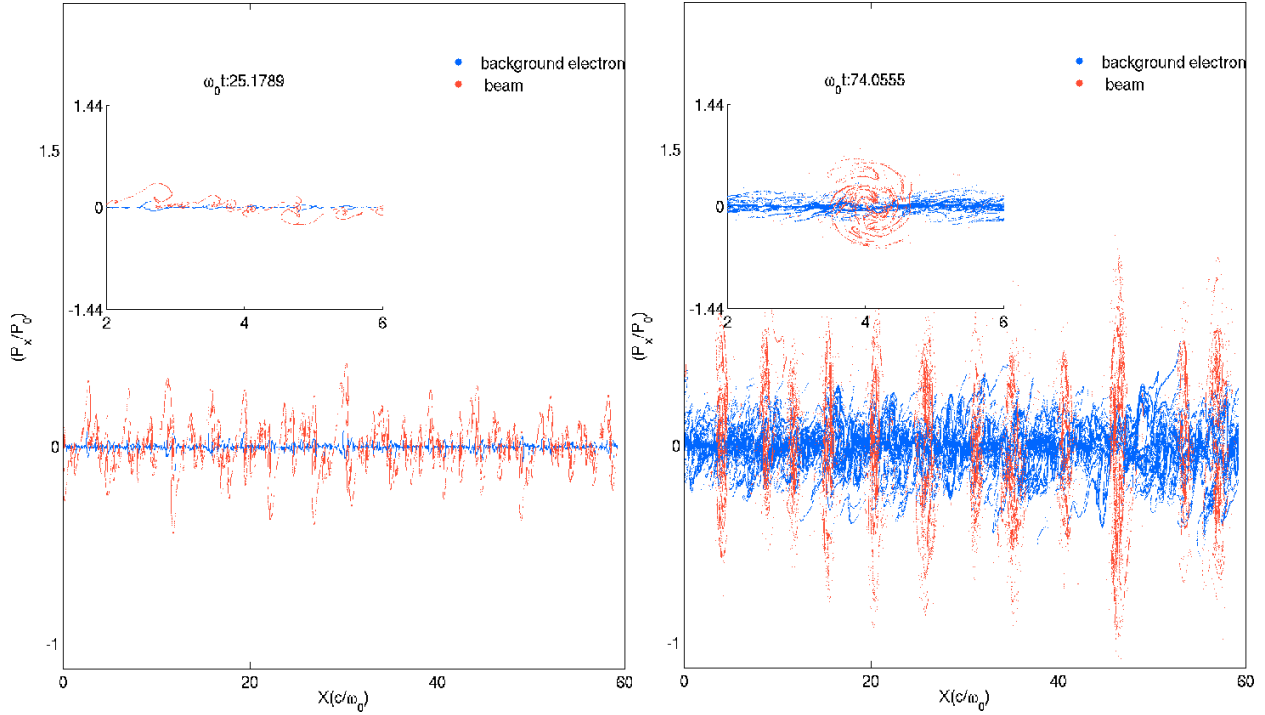


FIG. 6: projection of  $f(x, p_x)$  for homogeneous cold beam plasma at  $\omega_0 t=25.1789$  and  $74.0555$

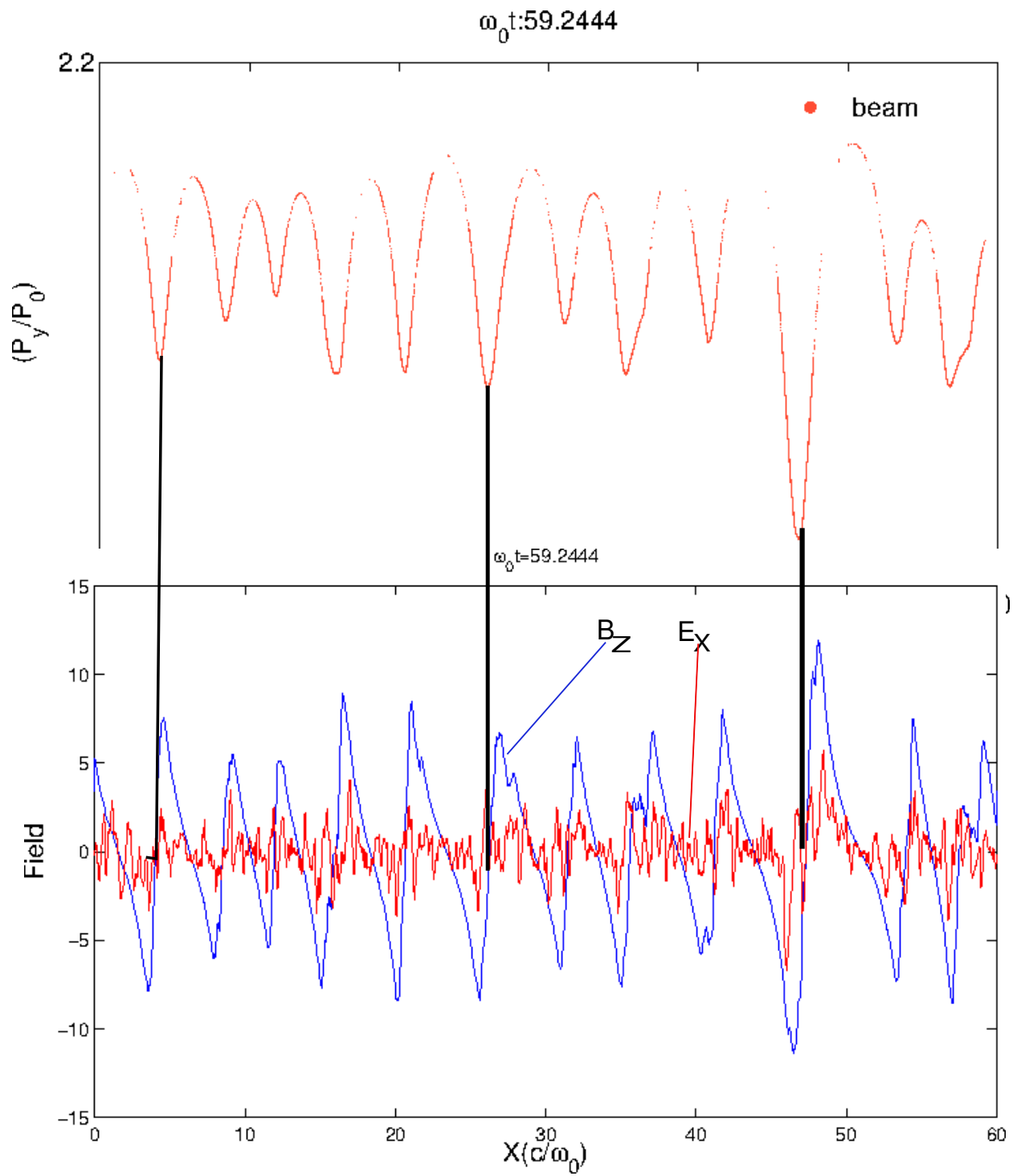


FIG. 7: Bunching of perturbed electron

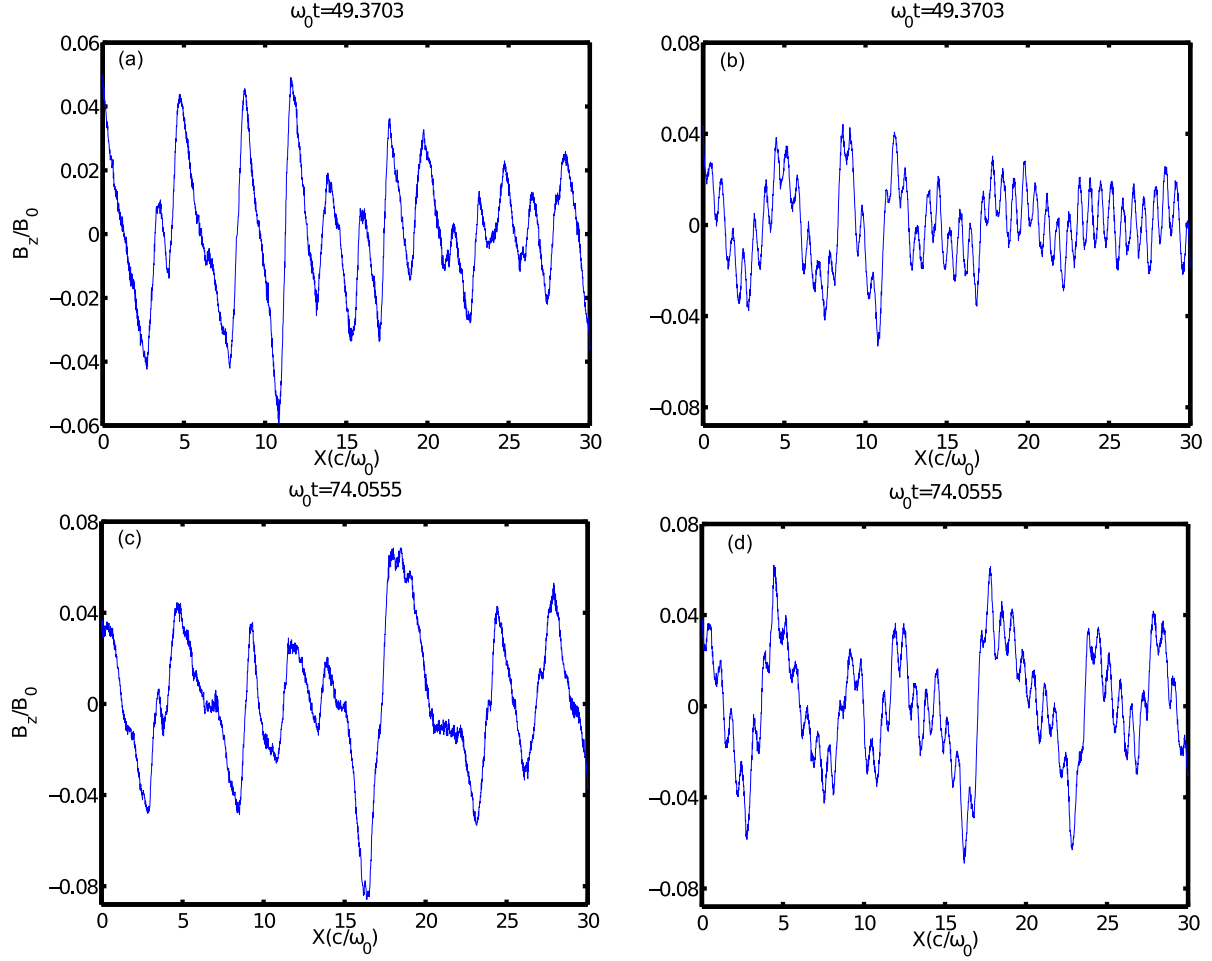


FIG. 8: spatial configuration of normalized magnetic field homogeneous and inhomogeneous hot beam plasma (a)  $\varepsilon=0.0$ ,  $k_s=0$  at  $\omega_0 t=49.3703$  (b)  $\varepsilon=0.2$ ,  $k_s=3\pi$  at  $\omega_0 t=49.3703$  (c)  $\varepsilon=0.0$ ,  $k_s=0$  at  $\omega_0 t=74.0555$  (d)  $\varepsilon=0.2$ ,  $k_s=3\pi$  at  $\omega_0 t=74.0555$

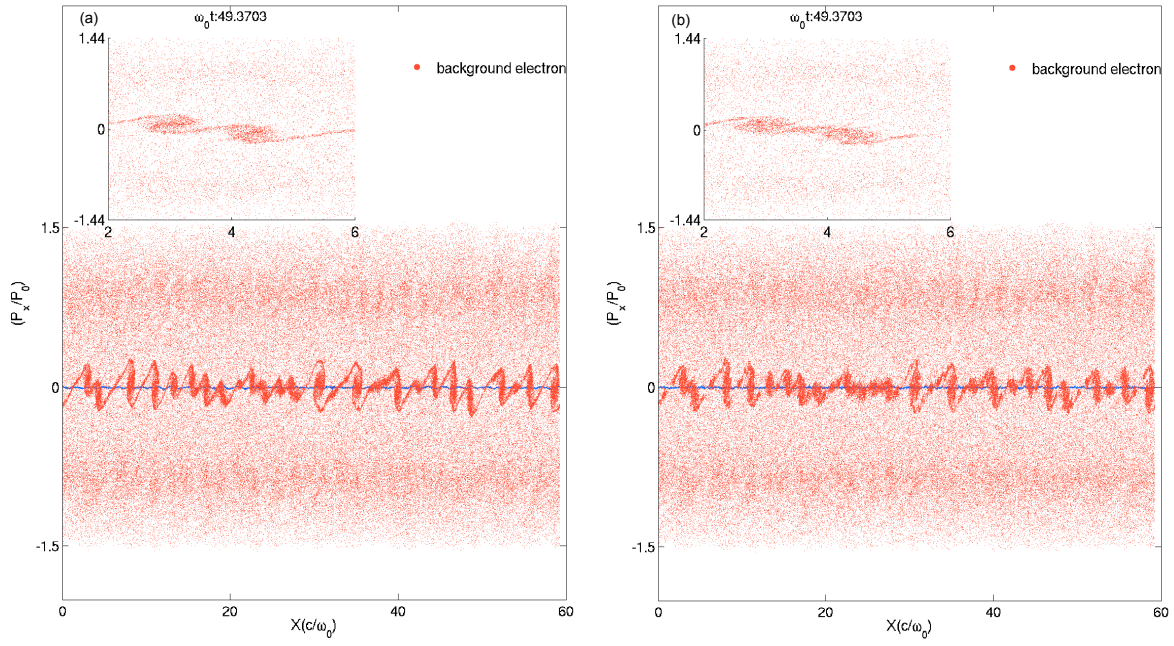


FIG. 9: projection of  $f(x, p_x)$  for warm system (a) beam with  $\varepsilon=0.0$ ,  $k_s=0$  at  $\omega_0 t=49.3703$   
 (b) beam with  $\varepsilon=0.2$ ,  $k_s=3\pi$  at  $\omega_0 t=49.3703$